

# Recoverability Estimation and Control for an Inverted Pendulum Walker Model Under Foot Slip

Marko Mihalec, Ye Zhao, and Jingang Yi

**Abstract**—Locomotion on low-friction surfaces is one of the most challenging problems for bipedal walking. When a stance foot moves and slips on the ground surface, the walker tries to determine whether it is feasible to avoid falling and continue walking. This study uses a simplified two-mass linear inverted pendulum model to analyze the biped dynamics under foot-slip conditions while maintaining closed-form solutions. Using the model, we analytically calculate safe, recoverable, and falling sets to determine whether the walker is able to recover towards a stable position or the fall is inevitable. We present a set of configurations which partition state space and determine the recoverability of the walker. A simple center-of-mass controller is introduced to re-gain the stability by allowing the walker to recover from fall-prone configurations. One attractive property of the developed closed-form expressions lies in feasibility for real-time implementation as a basis for a high-level robust slip recovery controller.

## I. INTRODUCTION

Walking on a slippery surface presents a major challenge for biped walkers as it poses a risk for foot slip and subsequent fall. Fall-induced injuries rank the second largest contributor for economic burden for human walkers in the US [1] and the largest when it comes to elderly [2]. It becomes imperative to develop an effective modeling framework and predict slipping behaviors for fall-recovery control. Numerous clinical studies have been conducted for locomotion on slippery surfaces (e.g., [3]). Slip often occurs on the stance leg immediately after the heel-strike and it can be triggered as a result of change in terrain conditions [4]. The work in [5] present the parameters contributing towards the onset of slip and predicting fall motion. To complement the clinical studies, several models are presented to focus on the slip of the stance foot immediately following a heel-strike and analyze the simplified locomotion for recovery quantification [6]–[8]. The slip experiments also include the studies of shoe-ground interactions and wearable sensor-based real-time slip detection [9], [10].

Simple models prove to be effective for capturing dynamical behaviors of a biped walker. One well-received model in the field is the linear inverted pendulum model (LIPM) [11]. This model consists of a single massless telescopic leg and a single mass at the center-of-mass (CoM)

and maintains a constant CoM height. Variants of the LIPM have been reported and however all of them assume the mass concentrated in a single point as well as a stationary foot-ground contact. To relax the stationary foot assumption, the mass ought to be not centered in a single point. A two-mass model is presented in [12] to allow explicit modeling of foot slip. The linear two-mass model yields a solution in a closed form and it however does not allow the CoM to move vertically. In [13], a non-linear model is presented to capture both the horizontal and the vertical motion of the CoM. However, the work in [13] is only capable to numerically predict the stability region under slip and it is infeasible to be used to analyze and predict the stable regions.

One primary goal of stability analysis for a biped walker is to determine whether regaining stability is feasible under foot slip, and if feasible, to further design the appropriate control law to achieve a stable locomotion. Stability of a biped walker is defined by various measures, including the prominent one named as capture point [14], [15]. Built on the concept of capturability, the results in [16] have shown that two steps are sufficient for recovery under perturbation. In addition to foot placement, stability can also be quantified in terms of states to avoid a fall. The work in [17] present a set of safe states and the optimal control algorithms using a phase space manifold concept, whilst the study in [18] shows the effects of different models on biped walk stability.

The work presented in this paper is built on the ideas of capturability and recoverable sets and also the phase-space manifold for walking locomotion. We first extend the two-mass LIPM that was originally discussed in [12]. The stability and recovery regions are then proposed in the phase-space manifold and the corresponding slip-recovery control strategies are then discussed. We mainly focus on the stability analyses and slip-recovery control design. The main contributions of this work are twofold. We derive closed-form solutions of the safety and recoverability sets for both non-slip and slip locomotion scenarios, which has not been reported previously. Second, the work provide a systematic design of slip-recovery strategies on how to plan foot placements and timing of the recovery step to regain stability under foot slip perturbation.

## II. DYNAMICS MODELS AND SOLUTION MANIFOLDS

In this section, we mainly introduce a two-dimensional (2D) two-mass LIMP, similar to the one presented in [12]. Fig. 1 shows the schematic of the revised LIPM. The large mass  $m_1$  is located at a constant height  $z_c$  above the ground

This work was supported in part by US National Science Foundation award CMMI-1762556.

M. Mihalec and J. Yi are with Department of Mechanical and Aerospace Engineering, Rutgers University, Piscataway, NJ 08854 USA (email: marko.mihalec@rutgers.edu, jgyi@rutgers.edu).

Y. Zhao is with the Woodruff School of Mechanical Engineering, Georgia Institute of Technology, Atlanta, GA 30332 USA (email: ye.zhao@me.gatech.edu).

and represents the center of mass of the biped walker, while  $m_2$  stands for the lower leg mass and does not move on the ground during normal walking. The 2D location of the mass  $m_1$  is denoted by  $(x_c, z_c)$  in the inertial frame, and  $x_f$  denotes the position of the foot contact point. At the contact point, the ground reaction forces are denoted by  $F_x$  and  $F_y$  in the horizontal and vertical directions, respectively. The model includes the ankle torque actuation, which is modeled equivalently as a change in the center-of-pressure (CoP) of the walker. Variable  $u$  denotes the absolute CoP position in the inertial frame. We also define  $u_r$  as a distance of  $u$  from the foot contact point, that is,  $u_r = x_f - u$ . Note that in the case of unactuated system, we have  $u_r = 0$ , i.e.,  $u = x_f$ . Ankle torque has an upper limit and equivalently it results in  $|u_r| \leq u_r^{\max}$ , where  $u_r^{\max}$  is the maximum actuation bound.

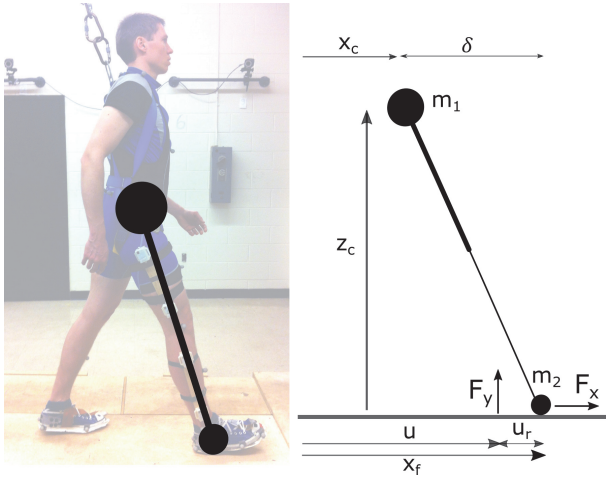


Fig. 1. Left: LIP model as related to human walker. Right: Details of a two mass LIP model.

The governing dynamics equation for the moment balance is derived and written as [12]

$$\ddot{x}_c - \ddot{x}_f = \frac{r_2}{z_c}(x_c - u) + \frac{r_1 g}{z_c}u_r - \frac{F_x}{m_2}, \quad (1)$$

where  $F_x = m_1 \ddot{x}_c + m_2 \ddot{x}_f$ ,  $r_1 = \frac{m_1 + m_2}{m_1}$  and  $r_2 = \frac{m_1 + m_2}{m_2}$ , i.e.,  $\frac{1}{r_1} + \frac{1}{r_2} = 1$ . By introducing  $\delta = x_c - x_f$  and under the assumption of no foot slip, that is,  $\dot{x}_f = \ddot{x}_f = 0$  and  $F_x = m_1 \ddot{x}_c$ , we have

$$\ddot{\delta} = \omega_n^2(\delta + r_1 u_r), \quad (2)$$

where  $\omega_n = \sqrt{\frac{g}{z_c}}$ . For slip case, we assume the friction relationship as  $F_x = \mu F_y$ , where  $\mu$  is the friction coefficient, and then Eq. (1) becomes

$$\ddot{\delta} = \omega_s^2(\delta + r_1 u_r + \mu z_c). \quad (3)$$

where  $\omega_s = \sqrt{\frac{r_2 g}{z_c}}$ . We next aim to solve the above dynamic equations and derive the phase-space manifolds on which the solutions reside. We consider the following three distinct cases: (i) no foot slip, (ii) a general contact where slipping acceleration is treated as a parameter, and (iii) a Coulomb friction is considered.

For non-slip case, the reduced-order dynamics is obtained from (2) and we consider the solution under a constant  $u_r = u_{r0}$  (constant) case, namely,

$$\ddot{\delta} = \omega_n^2(\delta + r_1 u_{r0}).$$

With initial conditions  $\delta_0$  and  $\dot{\delta}_0$ , the solution of the above equation is obtained as  $\delta(t) = \frac{\dot{\delta}_0}{\omega_n} \sinh(\omega_n t) + \delta_0 \cosh(\omega_n t) - r_1 u_{r0}$ . The solution manifold in the  $\delta$ - $\dot{\delta}$  space is obtained as

$$\mathcal{M}_n : \sigma = (\delta^2 - \delta_0^2)\omega_n^2 + \dot{\delta}_0^2 - \dot{\delta}^2 + 2\omega_n^2(\delta - \delta_0)r_1 u_{r0}. \quad (4)$$

Note that  $\sigma = 0$  represents the nominal system dynamics in the  $\delta$ - $\dot{\delta}$  state space. Non-zero  $\sigma$  denotes a deviation from the manifold  $\mathcal{M}_n$  and  $\sigma$  represents the Riemannian distance to  $\mathcal{M}_n$  [17].

To generalize the above results to foot slip case, we treat acceleration  $\ddot{x}_f$  as a parameter and no friction model is explicitly used. In the actuation-free case (i.e.,  $u_r = 0$ ), Eq. (1) is rewritten as

$$\ddot{\delta} = \omega_n^2 \delta - \ddot{x}_f,$$

where we express and use force  $F_x = m_1 \ddot{\delta} + (m_1 + m_2) \ddot{x}_f$  to obtain the above equation. The invariant manifold of this system is derived as:

$$\delta^2 \omega_n^2 + \dot{\delta}_0^2 + 2\delta_0 \ddot{x}_f = \delta_0^2 \omega_n^2 + \dot{\delta}^2 + 2\delta \ddot{x}_f \quad (5)$$

The manifold in (5) represents the generalized version of the one given by (4) since the latter can be derived from the former by non-slip conditions.

For slip case with friction coefficient  $\mu$ , we consider a constant control input  $u_r = u_{r0}$  and rewrite (3) as

$$\ddot{\delta} = \omega_s^2(\delta + \mu z_c + r_1 u_{r0}), \quad (6)$$

Similar to the first case, we obtain an analytical solution  $\delta(t) = \frac{\dot{\delta}_0}{\omega_s} \sinh(\omega_s t) + (\delta_0 + \mu z_c) \cosh(\omega_s t) - \mu z_c - r_1 u_{r0}$  with initial conditions and then the manifold

$$\mathcal{M}_s : \sigma = (\delta^2 - \delta_0^2)\omega_s^2 + \dot{\delta}_0^2 - \dot{\delta}^2 + 2\omega_s^2(\delta - \delta_0)(\mu z_c + r_1 u_{r0}). \quad (7)$$

Similarly, manifold  $\mathcal{M}_s$  defined by  $\sigma$  in (7) represents the Riemannian distance to the estimated locomotion trajectory under foot slip.

### III. RECOVERABILITY QUANTIFICATION

In this section, we present stability and recoverability sets by using the phase-space manifolds that are defined in the previous section.

We first introduce and extend the phase-space manifold plot that is developed in [17] for non-slip walking to foot slip case. Fig. 2 illustrates the phase portrait of the relative CoM motion dynamics in the  $\delta$ - $\dot{\delta}$  plane. We visualize and plot the phase-space manifolds and therefore characterize the stability and design slip-recovery strategies. Without a loss of generality, we assume that the walker moves in the positive  $x$  direction, i.e., the right-side movement. At the

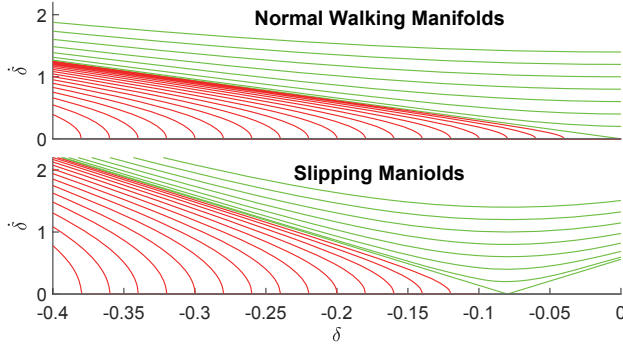


Fig. 2. Invariant manifolds ( $u_r = 0$ ) in the  $\delta$ - $\dot{\delta}$  space for normal walking  $\mathcal{M}_n$  (top) and slipping  $\mathcal{M}_s$  (bottom) gait. The manifolds can be partitioned into safe, denoted by green and falling, denoted by red.

onset of slip, the configuration of the initial state is defined with  $\dot{x}_c, \dot{x}_f > 0$  and  $\delta < 0$ , that is,  $x_c < x_f$ .

In the  $\delta$ - $\dot{\delta}$  plane, we partition the phase-space manifold plot (i.e.,  $\sigma$  curves shown in Fig. 2) safe and falling manifolds that are characterized by  $\dot{\delta} > 0$  and  $\dot{\delta} < 0$ , respectively. The separation curve between the safe and falling manifolds are particularly helpful to identify the stable, recoverable and fall-prone sets in the phase-space plane that will be defined later in this section. We denote the separation curve in the second quadrant of the  $\delta$ - $\dot{\delta}$  plane as  $\mathcal{B}$ .

To clearly describe the different regions in the  $\delta$ - $\dot{\delta}$  plane, we introduce the different boundaries. Let us first define points set  $\mathcal{C}_s = \{(\delta, \dot{\delta}) : \delta = 0, \dot{\delta} \geq 0\}$ . To facilitate the following presentation, we also define the safety region  $\mathcal{R}_s = \{(\delta, \dot{\delta}) : \dot{\delta} \geq 0\}$ . We define the regions  $\mathcal{R}_i^j$  in the  $\delta$ - $\dot{\delta}$  plane, where the subscribe  $i = \text{sl}, n$  stands for foot slip and normal walking locomotion and superscript  $i = \text{s}, r, f$  represents stable, recoverable and fall-prone regions, respectively.

**Definition 1:** For the flow governed by non-slip dynamics (2) (or (3) for slip case), a *stable region*  $\mathcal{R}_n^s \subset \mathcal{R}_s$  ( $\mathcal{R}_{\text{sl}}^s \subset \mathcal{R}_s$ ) for normal (slip) walking is the region that there exists time  $t_1 \geq 0$  with  $u_r \equiv 0$ , point  $(\delta(t_1), \dot{\delta}(t_1)) \in \mathcal{C}_s$ ; a *recoverable region*  $\mathcal{R}_n^r$  ( $\mathcal{R}_{\text{sl}}^r$ ) is defined as the *largest* region that there exists time  $t_1 \geq 0$  and  $u_r \neq 0$ , point  $(\delta(t_1), \dot{\delta}(t_1)) \in \mathcal{C}_s$ ; a *fall-prone region*  $\mathcal{R}_n^f$  ( $\mathcal{R}_{\text{sl}}^f$ ) is the region that does belong to either  $\mathcal{R}_n^s$  ( $\mathcal{R}_{\text{sl}}^s$ ) or  $\mathcal{R}_n^r$  ( $\mathcal{R}_{\text{sl}}^r$ ) in  $\mathcal{R}_s$ .

Fig. 3 illustrates these regions, that is, the green, yellow, and red areas represent  $\mathcal{R}_n^s \subset \mathcal{R}_s$  ( $\mathcal{R}_{\text{sl}}^s \subset \mathcal{R}_s$ ),  $\mathcal{R}_n^r$  ( $\mathcal{R}_{\text{sl}}^r$ ), and  $\mathcal{R}_n^f$  ( $\mathcal{R}_{\text{sl}}^f$ ), respectively. Note that fall-prone regions  $\mathcal{R}_n^f$  and  $\mathcal{R}_{\text{sl}}^f$  do not represent the fall states. Instead, these regions represent the states in which, without the intervention of taking a step, the locomotion can lead towards falling, regardless of the control input  $u_r$ .

It is clear from the above definition that recoverable region  $\mathcal{R}_n^r$  ( $\mathcal{R}_{\text{sl}}^r$ ) depends on control input  $u_r$ . Following the Pontryagin's minimum principle [19], we have the following results.

**Proposition 1:** The recoverable region  $\mathcal{R}_n^r$  ( $\mathcal{R}_{\text{sl}}^r$ ) under normal (slip) walking locomotion is given under the control

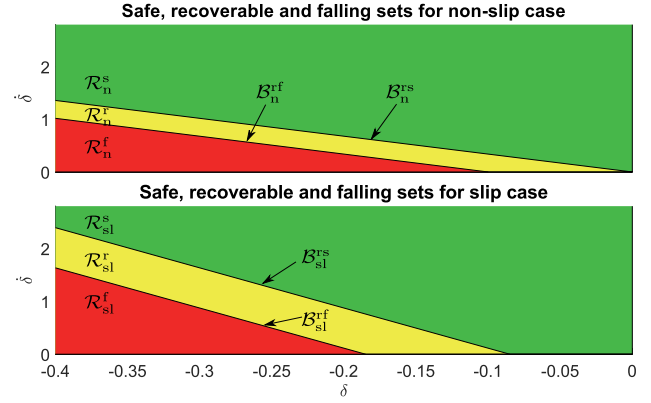


Fig. 3. Recoverability regions: Green:  $\mathcal{R}_i^s$  - stable, Yellow:  $\mathcal{R}_i^r$  - recoverable without taking a step, Red:  $\mathcal{R}_i^f$  - requires a walking step to recover.

input  $u_r^{\max}$ .

We omit the proof details of Proposition 1 due to page limit. With the above results, we define the separation boundary lines among two adjacent regions as follow.

**Definition 2:** A separation line in the phase plane, denoted as  $\mathcal{B}_n^j$  ( $\mathcal{B}_{\text{sl}}^j$ ),  $j = \text{rf}, \text{rs}$ , is defined as the boundary of two adjacent regions  $\mathcal{R}_n^r$  ( $\mathcal{R}_{\text{sl}}^r$ ) and  $\mathcal{R}_n^f$  ( $\mathcal{R}_{\text{sl}}^f$ ) and  $\mathcal{R}_n^s$  ( $\mathcal{R}_{\text{sl}}^s$ ), respectively. Therefore,  $\mathcal{B}_i^{\text{rf}} = \mathcal{R}_i^r \cap \mathcal{R}_i^f$  and  $\mathcal{B}_i^{\text{rs}} = \mathcal{R}_i^r \cap \mathcal{R}_i^s$ ,  $i = n, \text{sl}$ .

Fig. 3 illustrates these separation lines. We are now ready to compute the analytical forms for  $\mathcal{B}_n^j$  ( $\mathcal{B}_{\text{sl}}^j$ ),  $j = \text{rf}, \text{rs}$ , for normal (foot-slip) walking locomotion.

For  $\mathcal{B}_n^{\text{rf}}$ , considering manifold  $\mathcal{M}_n$  in (4), by Proposition 1, we enforce  $u_{r0} = u_r^{\max}$  and  $\sigma = 0$  and then obtain the hyperbolic curve for the set of manifolds in the  $\delta$ - $\dot{\delta}$  plane as

$$(\delta + r_1 u_r^{\max})^2 - \frac{\dot{\delta}^2}{\omega_n^2} = (\delta_0 + r_1 u_r^{\max})^2 - \frac{\dot{\delta}_0^2}{\omega_n^2}. \quad (8)$$

It is straightforward to obtain that the asymptote in the second quadrant is given by

$$\mathcal{B}_n^{\text{rf}}: \quad \dot{\delta} + \omega_n \delta = -\omega_n r_1 u_r^{\max}. \quad (9)$$

Similarly, by setting  $u_{r0} = 0$  we calculate the asymptote for  $\mathcal{B}_n^{\text{rs}}$  as

$$\mathcal{B}_n^{\text{rs}}: \quad \dot{\delta} + \omega_n \delta = 0. \quad (10)$$

To compute  $\mathcal{B}_{\text{sl}}^{\text{rf}}$  and  $\mathcal{B}_{\text{sl}}^{\text{rs}}$ , we take the manifold  $\mathcal{M}_s$  in (7) and obtain the hyperbolic curve as

$$(\delta + \mu z_c + r_1 u_{r0})^2 - \frac{\dot{\delta}^2}{\omega_s^2} = (\delta_0 + \mu z_c + r_1 u_{r0})^2 - \frac{\dot{\delta}_0^2}{\omega_s^2}. \quad (11)$$

By setting  $u_{r0} = u_r^{\max}$  and 0 in (11), we obtain them respectively as

$$\mathcal{B}_{\text{sl}}^{\text{rf}}: \quad \dot{\delta} + \omega_s \delta = -\omega_s (\mu z_c + r_1 u_r^{\max}), \quad (12)$$

$$\mathcal{B}_{\text{sl}}^{\text{rs}}: \quad \dot{\delta} + \omega_s \delta = -\omega_s \mu z_c. \quad (13)$$

Fig. 4 illustrates all boundary lines in the phase plane. It is clear from (9)-(13) that lines  $\mathcal{B}_{\text{sl}}^{\text{rf}}$  ( $\mathcal{B}_n^{\text{rf}}$ ) are parallel each

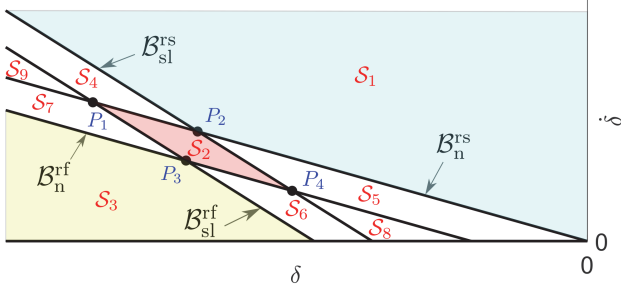


Fig. 4. An overlapping view of the recoverability regions for slip and non-slip cases highlighting the relationships between boundaries  $\mathcal{B}_i^r$  and the intersection  $P$

other with  $\mathcal{B}_{sl}^{rs}$  ( $\mathcal{B}_n^{rs}$ ). Moreover, the slope  $\omega_s > \omega_n$  and these lines intersect at four points, denoted as  $P_1 = \mathcal{B}_{sl}^{rs} \cap \mathcal{B}_n^{rf}$ ,  $P_2 = \mathcal{B}_{sl}^{rs} \cap \mathcal{B}_n^{rs}$ ,  $P_3 = \mathcal{B}_{sl}^{rf} \cap \mathcal{B}_n^{rf}$ , and  $P_4 = \mathcal{B}_{sl}^{rf} \cap \mathcal{B}_n^{rs}$ ; see Fig. 4. The coordinates for these four points are

$$\begin{aligned} P_1 &(-r_\omega(\mu z_c + r_1 u_r^{\max}), r_\omega \omega_n(\mu z_c + r_1 u_r^{\max})), \\ P_2 &(-r_\omega \mu z_c, r_\omega \omega_n \mu z_c), \\ P_3 &(-r_\omega \mu z_c - r_1 u_r^{\max}, r_\omega \omega_n \mu z_c), \\ P_4 &(-r_\omega(\mu z_c - r_1 u_r^{\max}/\sqrt{r_2}), r_\omega \omega_n(\mu z_c - r_1 u_r^{\max})), \end{aligned}$$

where  $r_\omega = \frac{\omega_s}{\omega_s - \omega_n} > 1$ . Since all the constants are positive we can determine by inspection that  $P_1$ ,  $P_2$ , and  $P_3$  always lie above the abscissa  $\dot{\delta} = 0$ , while point  $P_4$  can be on the line of  $\dot{\delta} = 0$  when the parameters are such that  $\mu z_c = r_1 u_r^{\max}$ .

Two pairs of parallel boundary lines indeed partitions the second quadrant of the phase plane into nine sets, denoted as  $\mathcal{S}_1, \dots, \mathcal{S}_9$  as shown in Fig. 4. Note that  $P_4$  represents the upper limit of intersection region  $\mathcal{S}_8 = \mathcal{R}_n^f \cap \mathcal{R}_{sl}^s$ . Therefore, when  $P_4$  lies below the line  $\dot{\delta} = 0$ , the two regions do not intersect, that is, region  $\mathcal{S}_8$  does not exist. In other words, if  $\mu z_c \leq r_1 u_r^{\max}$ , keeping the model within  $\mathcal{R}_{sl}^s$  becomes a sufficient condition to avoid both fall-prone regions  $\mathcal{R}_{sl}^f$  and  $\mathcal{R}_n^f$ . This observation is helpful for recovery strategies in the next section.

Depending on the location of state  $\mathbf{x}(t) = [\delta(t) \ \dot{\delta}(t)]^T$  in the regions in the  $\delta$ - $\dot{\delta}$  plane at the onset of slip, the slip recovery strategies can be different. If  $\mathbf{x}(t)$  is within certain regions, a torque control within the same step should be used to maintain the balance, while in other regions, additional recovery step must be initiated to possibly recover from slip-induced fall risk. In the next section, we will present the recovery control within one step and foot placement location and time if one slip-recovery step is needed.

#### IV. SLIP RECOVERY CONTROL

##### A. Within-Step and One-Step Recovery Control

We present recovery control strategies using the regions defined in the previous section. The advantage of the previous analysis and the simplified model with explicit solutions helps to formulate simple controllers that do not need any prediction horizon and can be implemented in real time. The objective of slip-recovery control is to determine the action to maintain balance depending on where the current state  $\mathbf{x}(t)$  is located in the phase plane.

1) *Stable region control*: In this case, the walker current state is in one of the stable regions  $\mathbf{x} \in \mathcal{R}_n^s$  ( $\mathcal{R}_{sl}^s$ ) for normal (slip) walking gaits. We here focus on actuation to keep balance and avoid slip-induced fall, and any additional actuation for walk gait progression is not explicitly addressed. Therefore, the controller is formulated to reach the desired state  $\mathbf{x}^d = [\delta^d \ \dot{\delta}^d]^T \in \mathcal{R}_n^s$  ( $\mathcal{R}_{sl}^s$ ). The desired state can lead to return to periodic walking, stopping or other stable gaits. The exact choice of  $\mathbf{x}^d$  depends on the desired task and is outside of the scope of this paper. For normal walking case,  $\dot{x}_f = 0$ , the desired state  $\mathbf{x}^d$  is on manifold  $\mathcal{M}_n^d$  that is defined by (4) with  $\delta_0 = \delta^d$ ,  $\dot{\delta} = \dot{\delta}^d$  and  $\sigma = 0$ , that is,

$$\mathcal{M}_n^d : \dot{\delta}^2 - (\dot{\delta}^d)^2 = (\delta^2 - (\delta^d)^2)\omega_n^2 + 2\omega_n^2(\delta - \delta^d)r_1 u_{r0}.$$

Solving the above equation for  $u_{r0}$  yields the (constant) control input as

$$u_{r0} = \frac{\dot{\delta}^2 - (\dot{\delta}^d)^2 - (\delta^2 - (\delta^d)^2)\omega_n^2}{2\omega_n^2(\delta - \delta^d)r_1}. \quad (14)$$

Similarly, for the slip case  $\dot{x}_f \neq 0$ , we use (7) to obtain the desired manifold  $\mathcal{M}_s^d : \dot{\delta}^2 - (\dot{\delta}^d)^2 = (\delta^2 - (\delta^d)^2)\omega_s^2 + 2\omega_s^2(\delta - \delta^d)(\mu z_c + r_1 u_{r0})$ , and control input  $u_{r0}$  for slip case as

$$u_{r0} = \frac{\dot{\delta}^2 - \dot{\delta}^d{}^2 - (\delta^2 - \delta^d{}^2)\omega_s^2}{2\omega_s^2(\delta - \delta^d)r_1} - \frac{\mu z_c}{r_1}. \quad (15)$$

2) *Recoverable region control*: If the state  $\mathbf{x} \in \mathcal{R}_n^f$  ( $\mathcal{R}_{sl}^f$ ) for normal (slip) walking gaits, recovery is feasible without taking an additional recovery step. However, without actuation the gait leads to a fall and therefore, the control goal in this case is to leave the recoverable regions  $\mathcal{R}_n^f$  or  $\mathcal{R}_{sl}^f$  as quick as possible. Note that to reach the safe regions  $\mathcal{R}_n^s$  or  $\mathcal{R}_{sl}^s$ , the walker must get in  $\mathcal{B}_n^{rs}$  ( $\mathcal{B}_{sl}^{rs}$ ) for normal (foot-slip) walk gaits. Therefore, the design objective is to minimize the Reimanian distance  $\sigma$  from  $\mathcal{B}_n^{rs}$  or  $\mathcal{B}_{sl}^{rs}$  given by (4) or (7) for normal or slip walking gaits, respectively, with  $\mathbf{x}_0 \in \mathcal{B}_n^{rs}$  ( $\mathcal{B}_{sl}^{rs}$ ).

We obtain the minimum required control actuation to return from the recoverable to the stable regions in normal walking case by using (14) with  $\mathbf{x}^d = \mathbf{0} \in \mathcal{B}_n^{rs}$

$$u_{r0} = \frac{\dot{\delta}^2 - \delta^2 \omega_n^2}{2\omega_n^2 \delta r_1}.$$

Since the above  $u_{r0}$  represents the minimum admissible control input for recovery, we assume that  $u_{r0} \leq u_r^{\max}$  and under such control, it takes longer time to reach stable region and is also vulnerable to any perturbations. To increase robustness and guarantee the recovery in the shortest time, we propose the use of bang-bang control to allow the maximum control effort

$$u_{r0} = u_r^{\max}.$$

By the results in Proposition 1, the above control guarantees that the walker recovers from any possible state within  $\mathcal{R}_n^f$  ( $\mathcal{R}_{sl}^f$ ).

3) *Fall-prone region control*: A walker in the fall prone regions  $\mathbf{x} \in \mathcal{R}_n^f(\mathcal{R}_{sl}^f)$  for  $\dot{x}_f = 0$  ( $\dot{x}_f \neq 0$ ) cannot maintain balance with any possible  $u_r(t)$  and therefore, additional recovery steps must be taken. To use the additional recovery step, we need to determine foot placement location and timing to avoid a fall.

In this work, a step is treated as an instantaneous change in stance foot location, while velocities  $\dot{x}_c$ ,  $\dot{x}_f$  and  $\dot{\delta}$  are assumed to be continuous before and after taking the step, that is,  $\dot{\delta}_n(t_f) = \dot{\delta}_{n+1}(0)$ , where  $n$  and  $n+1$  denote the  $n$ th and  $(n+1)$ th steps, respectively, and  $t_f$  is the final time of the  $n$ th step. Therefore, taking a step results in an instantaneous change in  $\delta$ , namely,  $\delta_{n+1}(0) = \delta_n(t_f) + x_{st}$ , where  $x_{st}$  is the displacement of the foot placement behind the current stance at the  $n$ th step. By the above treatment, taking a step is represented by an horizontal jump from one point to another in the  $\delta$ - $\dot{\delta}$  phase plane.

For  $\mathbf{x} \in \mathcal{R}_n^f(\mathcal{R}_{sl}^f)$ , the goal of the recovery step is to bring the states back into safe regions  $\mathcal{R}_n^s(\mathcal{R}_{sl}^s)$ . The step  $x_{st}$  should result in a walker reaching a desired state  $\mathbf{x}^d$ . Since any  $\mathbf{x}^d \in \mathcal{R}_n^s(\mathcal{R}_{sl}^s)$  enables the walker into a safe region, we look for the minimal recovery step size and consider an  $\mathbf{x}^d \in \mathcal{B}_n^{rs}(\mathcal{B}_{sl}^{rs})$ . Furthermore, considering  $\delta^d = \dot{\delta}$  by the above step treatment and for a normal walking case,  $\delta^d$  can be obtained from (10), the foot placement is calculated as  $x_{st} = \delta^d - \delta$  and this yields

$$x_{st} = -\frac{\dot{\delta}}{\omega_n} - \delta.$$

For foot-slip case, Eq. (13) is used to obtain  $\delta^d$  and that yields

$$x_{st} = -\mu z_c - \frac{\dot{\delta}}{\omega_s} - \delta.$$

To determine the optimal time to take the recovery step under slip gait, we consider two manifolds  $\mathcal{M}_s^n$  and  $\mathcal{M}_s^{n+1}$  that correspond the  $n$ th and  $(n+1)$ th steps, respectively. The initial condition for  $\mathcal{M}_s^n$  is denoted by  $\mathbf{x}_0 = [\delta_0 \ \dot{\delta}_0]^T$  and for  $\mathcal{M}_s^{n+1}$ ,  $\mathbf{x}_0 + \Delta\mathbf{x}_0 = [\delta_0 + \Delta\delta_0 \ \dot{\delta}_0]^T$ . It is clear that a transition step between the two manifolds at  $t = 0$  has step length  $x_{st} = \Delta\delta_0$  (with no instantaneous velocity change). We consider the step length property for  $t \geq 0$  with the above initial conditions.

The progression difference, denoted by  $\Delta\delta(t)$ , represents the horizontal distance between manifolds  $\mathcal{M}_s^n$  and  $\mathcal{M}_s^{n+1}$ . We use (11) to compute  $\Delta\delta(t)$  under initial conditions  $\mathbf{x}_0$  and  $\mathbf{x}_0 + \Delta\mathbf{x}_0$ , respectively. Under these two sets of initial conditions, the expressions for  $\delta$  are denoted as  $\delta_{\mathbf{x}_0}$  and  $\delta_{\mathbf{x}_0 + \Delta\mathbf{x}_0}$ , respectively, and therefore, we obtain

$$\Delta\delta(t) = \delta_{\mathbf{x}_0} - \delta_{\mathbf{x}_0 + \Delta\mathbf{x}_0} = \sqrt{(\delta_0 + \mu z_c + r_1 u_{r0})^2 + \frac{\dot{\delta}^2 - \dot{\delta}_0^2}{\omega_s^2}} - \sqrt{(\delta_0 + \Delta\delta_0 + \mu z_c + r_1 u_{r0})^2 + \frac{\dot{\delta}^2 - \dot{\delta}_0^2}{\omega_s^2}}.$$

It is clear that  $\Delta\delta(t)$  is a function of velocity  $\dot{\delta}$  for a given initial condition value and constant control  $u_{r0}$ . Fig. 5

illustrates  $\Delta\delta$  as a function of velocity  $\dot{\delta}$ . Clearly,  $\Delta\delta$  is a monotonically decreasing function of  $\dot{\delta}$ . Indeed, we can show this by the fact that

$$\frac{d\Delta\delta}{d\dot{\delta}} = \frac{\dot{\delta}}{\omega_s^2} \left[ \frac{1}{\sqrt{(\delta_0 + \mu z_c + r_1 u_{r0})^2 + (\dot{\delta}^2 - \dot{\delta}_0^2)/\omega_s^2}} - \frac{1}{\sqrt{(\delta_0 + \Delta\delta_0 + \mu z_c + r_1 u_{r0})^2 + (\dot{\delta}^2 - \dot{\delta}_0^2)/\omega_s^2}} \right] < 0.$$

The last inequality in the above equation is obtained by the observation as follows. In the second quadrant of the  $\delta$ - $\dot{\delta}$  plane,  $\delta, \delta_0 < 0$  and  $\dot{\delta} > 0$ . For any  $\mathbf{x} \in \mathcal{R}_{sl}^f$ ,  $\delta + \mu z_c + r_1 u_{r0} < 0$ . Because of  $\Delta\delta_0 > 0$ , the second term in the above equation is always greater than the first one and therefore,  $d\Delta\delta/d\dot{\delta} < 0$ . From (6), for  $\mathbf{x} \in \mathcal{R}_{sl}^f$ ,  $\ddot{\delta}(t) < 0$  and by the chain rule, we obtain

$$\frac{d\Delta\delta}{dt} = \frac{d\Delta\delta}{d\dot{\delta}} \ddot{\delta}(t) > 0.$$

The above results imply that the progression difference required for transition between two manifolds increases with time, namely,  $\Delta\delta(t) > \Delta\delta_0$  for  $t > 0$ . Therefore, the ideal timing to take the recovery step is at  $t = 0$ , namely, as soon as possible once the slip is detected. Same conclusion can be obtained for normal walk manifold  $\mathcal{M}_n$ .

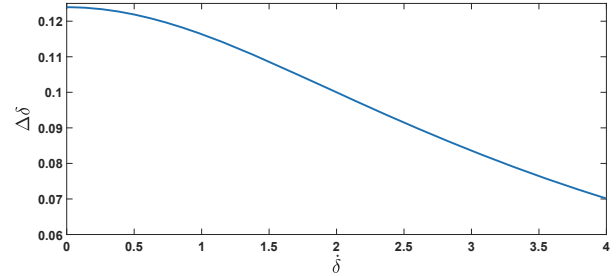


Fig. 5. Distance between two manifolds with different initial conditions.

### B. Illustrative Example

We demonstrate the above controller design through a simulation example. Fig. 6 shows a series of snapshot of a simulated walking gaits under slip. While the bipedal walker is model and visualized as a five-link structure, its CoM movement is governed by a two-mass LIPM presented in Section II. The values of the model parameters are chosen as  $m_1 = 65$  kg,  $m_2 = 5$  kg, and  $z_c = 1$  m. The movement starts as periodic walking gaits and the standing foot is in stationary contact with the ground (Fig. 6 (a)). During the continuous phase no actuation is applied, that is,  $u_r = 0$ . At the moment of heel strike, the model experiences instantaneous change in  $\delta$  and thus a horizontal jump in the  $\delta$ - $\dot{\delta}$  phase plane (Fig. 6 (b)). During periodic walking, the model never enters the  $\mathcal{R}_n^f$  region and due to the frictional condition changes, foot slip might occur at any time. When the slip occurs, the position of the state variables of the model remains unchanged, but the relevant boundary regions changes and thus, the walker states lie in the fall-prone

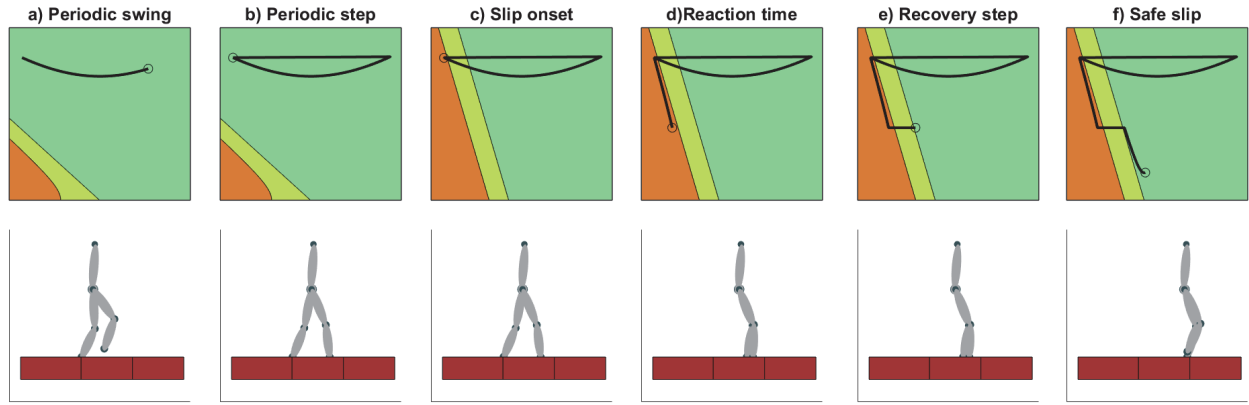


Fig. 6. Snapshot of a simulation sample: (a) Periodic walking swing phase. (b) A step during periodic walking. Steps are represented as horizontal jumps in the  $\delta$ - $\dot{\delta}$  phase plane. (c) Slip onset at the moment of heel-strike.  $\delta$  and  $\dot{\delta}$  remain unchanged and however the region limits  $\mathcal{B}_i^f$  and  $\mathcal{B}_i^s$  change from  $i = n$  to  $i = sl$ . (d) Slipping on the standing foot. The controlled action  $u_r^{\max}$  is applied. However, since the model is within the fall-prone set, a fall would occur unless a recovery step is taken. (e) Swing foot touches on the ground and that brings the model into the stable region. (f) The model continues slipping but remains within the stable region.

region  $\mathcal{R}_{sl}^f$  (Fig. 6 (c)). By definition,  $u_r^{\max}$  is insufficient for recovery so the model continues the progression on a fall prone manifold in  $\mathcal{R}_{sl}^f$  (Fig. 6 (d)) until a recovery step is taken (Fig. 6 (e)). The step results in an instantaneous change of  $\delta$  bringing the model to the safe region  $x \in \mathcal{R}_{sl}^s$  (Fig. 6 (e)). The walker then continues the progression safely despite its foot still slipping on the floor (Fig. 6 (f)).

## V. CONCLUSION

This paper extended the linear two-mass inverted pendulum model for normal walking to the foot-slip case. Analytical state-space manifolds have been derived to quantify various stability sets for controller design. It was shown that by using only the relative position and velocity between the foot and the CoM, the recovery feasibility sets was quantified. Depending on the set of current parameters, the walker's movement was characterized as safe, fall-prone or recoverable. We have shown that in the cases with large enough actuation capability, the safe region under slipping condition was sufficient for recovery under foot slip. Under certain fall-prone situations, a recovery step had to be taken such that the state moved back to a recoverable region. It was shown that such a step should be taken immediately and foot placement location was designed by using the model.

## REFERENCES

- [1] P. Corso, E. Finkelstein, T. Miller, I. Fiebelkorn, and E. Zaloshnja, "Incidence and lifetime costs of injuries in the United States," *Injury Prevent.*, vol. 12, no. 4, pp. 212–218, 2006.
- [2] S. Heinrich, K. Rapp, U. Rissmann, C. Becker, and H.-H. König, "Cost of falls in old age: a systematic review," *Osteoporosis Intl.*, vol. 21, no. 6, pp. 891–902, 2010.
- [3] A. J. Chambers and R. Cham, "Slip-related muscle activation patterns in the stance leg during walking," *Gait Posture*, vol. 25, no. 4, pp. 565–572, 2007.
- [4] M. S. Redfern, R. Cham, K. Giolo-Perczak, R. Grönqvist, M. Hirvonen, H. Lanshammar, C. Y.-C. Pai, and C. Power, "Biomechanics of slips," *Ergonomics*, vol. 44, no. 13, pp. 1138–1166, 2001.
- [5] F. Yang and Y.-C. Pai, "Can stability really predict an impending slip-related fall among older adults?" *J. Biomech.*, vol. 47, no. 16, pp. 3876–3881, 2014.
- [6] K. Chen, M. Trkov, J. Yi, Y. Zhang, T. Liu, and D. Song, "A robotic bipedal model for human walking with slips," in *Proc. IEEE Int. Conf. Robot. Autom.*, Seattle, WA, 2015, pp. 6301–6306.
- [7] K. Chen, M. Trkov, and J. Yi, "Hybrid zero dynamics of human walking with foot slip," in *Proc. Amer. Control Conf.*, Seattle, WA, 2017.
- [8] M. Trkov, K. Chen, and J. Yi, "Bipedal model and extended hybrid zero dynamics of human walking with foot slips," *ASME J. Computat. Nonlinear Dyn.*, vol. 14, no. 10, 2019, article 101002.
- [9] M. Trkov, J. Yi, T. Liu, and K. Li, "Shoe-floor interactions human walking with slips: Modeling and experiments," *ASME J. Biomech. Eng.*, vol. 140, no. 3, pp. 031 005–1–031 005–11, 2018.
- [10] M. Trkov, K. Chen, J. Yi, and T. Liu, "Inertial sensor-based slip detection in human walking," *IEEE Trans. Automat. Sci. Eng.*, vol. 17, no. 1, pp. 348–360, 2020.
- [11] S. Kajita, F. Kanehiro, K. Kaneko, K. Yokoi, and H. Hirukawa, "The 3d linear inverted pendulum mode: A simple modeling for a biped walking pattern generation," in *Proc. IEEE/RSJ Int. Conf. Intell. Robot. Syst.*, Osaka, Japan, 2001, pp. 239–246.
- [12] K. Chen, M. Trkov, S. Chen, J. Yi, and T. Liu, "Balance recovery control of human walking with foot slip," in *Proc. Amer. Control Conf.*, Boston, MA, 2016, pp. 4385–4390.
- [13] M. Mihalec and J. Yi, "Capturability of inverted pendulum gait model under slip conditions," in *Proc. ASME Dyn. Syst. Control Conf.*, Atlanta, GA, 2018, article DSCC2018-9203.
- [14] J. Pratt, J. Carff, S. Drakunov, and A. Goswami, "Capture point: A step toward humanoid push recovery," in *Proc. IEEE Int. Conf. Humanoid Robots*, Genova, Italy, 2006, pp. 200–207.
- [15] T. Koolen, T. de Boer, J. Reubla, A. Goswami, and J. Pratt, "Capturability-based analysis and control of legged locomotion, Part 1: Theory and application to three simple gait models," *Int. J. Robot. Res.*, vol. 31, no. 9, pp. 1094–1113, 2012.
- [16] P. Zaytsev, J. S. Hasaneini, and A. Ruina, "Two steps is enough: No need to plan far ahead for walking balance," in *Proc. IEEE Int. Conf. Robot. Autom.*, Seattle, WA, 2015, pp. 6295–6300.
- [17] Y. Zhao, B. R. Fernandez, and L. Sentis, "Robust optimal planning and control of non-periodic bipedal locomotion with a centroidal momentum model," *Int. J. Robot. Res.*, vol. 36, no. 11, pp. 1211–1242, 2017.
- [18] M. Posa, T. Koolen, and R. Tedrake, "Balancing and step recovery capturability via sums-of-squares optimization," in *Proc. Robotics: Sci. Syst.*, Cambridge, MA, 2017, pp. 12–16.
- [19] D. P. Bertsekas, *Dynamic Programming and Optimal Control*. Athena scientific Belmont, MA, 1995.